Journal of Materials Chemistry A

ROYAL SOCIETY OF CHEMISTRY

PAPER

View Article Online
View Journal

Cite this: DOI: 10.1039/d5ta07868g

In situ photo-Fenton-like reaction and oxygen evolution through polaron-mediated WO_3

Ardiansyah Taufik, *[a] Akira Yoko, *[ab] Chunli Han, [a] Wahyudiono,[c] Satoshi Ohara[d] and Tadafumi Adschiri*[ad]

The effective utilization of both electrons and holes in semiconductor-based photocatalysis is crucial for enhancing light-driven chemical reactions. However, the photocatalytic performance of WO_3 is limited by its low conduction band potential, which restricts its ability to generate reactive species such as superoxide radicals and to facilitate hydrogen production. Consequently, WO_3 primarily relies on holes for redox processes, reducing its overall photocatalytic efficiency. This paper proposes a novel strategy to simultaneously exploit both charge carriers by activating a photo-Fenton-like reaction driven by the polaronic phenomena of electrons (W^{5+} formation). Electrons are responsible for generating hydroxyl radicals (•OH), enabling the degradation of acid orange 7 dye with an activity ten times higher than that of the conventional Fenton reaction. Meanwhile, holes effectively drive the oxygen evolution reaction (OER), achieving an oxygen yield of 1.62 mmol g^{-1} h^{-1}. The polaronic behaviour of WO_3 was further optimized by accelerated supersaturation degree through protonation which enhances the surface properties and increases W^{5+} formation during light irradiation. This strategy led to approximately threefold enhancement in acid orange 7 degradation and a 2.3-fold increase in OER performance (3.66 mmol g^{-1} h^{-1}, one of the highest reported values). Overall, this study presents a new approach to optimizing charge carrier utilization in photocatalysis, offering a promising pathway toward more efficient and versatile semiconductor-based systems.

Received 25th September 2025
Accepted 6th January 2026

DOI: 10.1039/d5ta07868g

rsc.li/materials-a

1. Introduction

The photo-Fenton reaction has emerged as a promising solution for wastewater treatment due to its strong oxidative capability in decomposing a wide range of pollutants,[1] including synthetic dyes,[2,3] pharmaceuticals,[4] and radioactive waste.[5] This process involves the reaction of iron salts with hydrogen peroxide, generating highly reactive hydroxyl radicals (•OH) that act as powerful oxidizing agents. However, the practical application of the Fenton reaction faces a major limitation: the residual iron salts remain in the solution after the reaction and are difficult to recover, potentially causing secondary pollution in water sources.[6] To address this issue, researchers have explored immobilizing iron sources in the form of iron oxides/hydroxides or anchoring them onto various supports such as metal oxide semiconductors,[7,8] metal–organic frameworks (MOFs),[9] and carbon-based materials.[10] Despite these advances, iron leaching—particularly under acidic conditions—remains a significant challenge,[11,12] limiting the long-term stability and sustainability of the process.

Instead of focusing solely on stabilizing iron ions, a more promising strategy is to develop stable materials that can generate hydroxyl radicals (•OH) through interactions with H_2O_2. For instance, previous studies have reported that TiO_2 with a high concentration of Ti^{3+} defects can serve as effective candidates. However, these Ti^{3+} defect sites are not reversible, leading to gradual performance degradation over time.[13] Other materials such as CuO with Cu^{2+} (ref. 14) content and Mn_3O_4 (ref. 15) exhibit low stability for long term usage. In contrast, tungsten trioxide (WO_3) offers a more structurally stable[16] alternative with defect reversibility due to polaronic behavior where the photoexcited electron localizes on tungsten sites with the local structure distortion W^{6+} to W^{5+},[17,18] which is similar to Fe^{2+}/Fe^{3+} making it a promising material for sustained hydroxyl radical generation.

Moreover, the utilization of electrons to generate hydroxyl radicals (•OH) allows the holes in WO_3 to be more freely available for driving chemical reactions which enable WO_3 as a photo-Fenton like reaction as well as photocatalytic reaction. Several studies have reported that the holes in WO_3 can promote the Oxygen Evolution Reaction (OER) in the presence of electron scavengers such as Ag^+ and Fe^{3+}.[19] However, the

[a]WPI-Advanced Institute for Materials Research (WPI-AIMR), Tohoku University, 2-1-1 Katahira, Aoba-ku, Sendai, Miyagi 980-8577, Japan. E-mail: ardiansyah.taufik.d2@tohoku.ac.jp; tadafumi.ajiri.b1@tohoku.ac.jp; akira.yoko.c7@tohoku.ac.jp

[b]International Center for Synchrotron Radiation Innovation Smart (SRIS), Tohoku University, Aramaki Aza-Aoba, Aoba-ku, Sendai, 980-8572, Japan

[c]Department of Chemical Engineering, Institut Teknologi Sepuluh Nopember, Kampus ITS Sukolilo, Surabaya, 60111, Indonesia

[d]New Industry Creation Hatchery Center, Tohoku University, Sendai 980-8579, Japan

activation of the OER in these systems is limited due to the non-recyclable nature of the scavenging process. In contrast, in the photo-Fenton-like reaction using WO_3, the electron scavenging process is expected to be efficiently recyclable, which could lead to enhanced OER efficiency.

Therefore, in this study, the novel utilization of both charge carriers in the direct photo-Fenton-like reaction of WO_3 by acknowledging the polaronic behavior of WO_3 was investigated. Recently, interesting polaron behavior in small nanoparticles driven by lattice distortion is reported for metal oxides including particle size effects and surface heterogeneity of polaron,[20–23] and thus the nanoparticle synthesis of WO_3 is also expected to exploit polaronic behavior. The utilization of both charge carriers, electrons and holes, by the photo-Fenton-like reaction was monitored by wastewater removal for electrons and the oxygen evolution reaction for holes at the same time. Currently, the usage of the photo-Fenton-like reaction of WO_3 always requires iron support to activate the reactions[24,25] which are probably attributed to the inefficient polaron formation of WO_3. Therefore, in this study, the efficiency of the polaron formation was further optimized by understanding the growth of WO_3, which is controlled by the control of the protonation process, enabling us to understand the crystallization difference that affects the photo-Fenton like efficiency. This study will provide new insights into the utilization of WO_3 as a catalytic material for promoting chemical reactions.

2. Experimental details

2.1 WO_3 synthesis

Initially, 3.3 g of disodium tungstate dihydrate ($Na_2WO_4 \cdot 2H_2O$) (Fujifilm Wako Pure Chemical Co.) was dissolved in 200 mL of deionized water under continuous stirring with a magnetic stirrer. Once fully dissolved, the solution was protonated by adding varying amounts of 37% HCl (Fujifilm Wako Pure Chemical Co.). The protonation process was controlled by adjusting the volume of HCl to 15 mL, 30 mL, 60 mL, and 180 mL, and the corresponding proton concentrations ($[H^+]$) were 0.8, 1.6, 2.8 and 5.7 M (SI, (S1)), hereafter referred to as $[H^+] = 0.8$, $[H^+] = 1.6$, $[H^+] = 2.8$, and $[H^+] = 5.7$, respectively. The solution was stirred continuously for 12 hours at room temperature. After stirring, the precipitate was collected by centrifugation and washed with deionized water until the pH of the supernatant reached 4–5. The washed sample was then dried under vacuum at 60 °C for 12 hours. Finally, the dried products underwent annealing at 400 °C for 2 hours under an ambient air atmosphere, yielding the final WO_3 product.

2.2 Materials characterization

The morphology of the particles was investigated by transmission electron microscopy (JEM-2100Plus, JEOL, Japan). The crystal structure and crystallite size were determined using X-ray powder diffraction (XRD, Rigaku SmartLab 9MTP, Japan) with a Cu Kα ($\lambda = 1.5418$ Å) radiation source at 3° min^{-1}. The 2θ scanning range is 20–80°. The chemical states of the samples were investigated by X-ray photoelectron spectroscopy (XPS; PHI5600, ULVAC-PHI, Japan) which was performed using monochromatized X-rays of Al Kα with a 300 W power source, and the fitting of tungsten elements was conducted from 33 to 40 eV with Shirley baseline methods. The optical absorption was monitored by UV-vis-NIR spectroscopy (V-770TWK, JASCO, Japan) and the luminescence analysis was investigated with a fluorescence spectrophotometer (FL), F-2700 Hitachi High-Technologies, Japan. The local structure of WO_3 was further characterized by microscopic confocal Raman spectroscopy (HORIBA LabRAM HR-800, Japan) with an excitation wavelength of 532 nm. The defect analysis was then performed by electron paramagnetic resonance spectroscopy (EPR) (B Bruker BioSpin, Bruker, Germany).

2.3 Photo-Fenton like reaction

The photo-Fenton-like reaction was evaluated by monitoring the degradation of acid orange 7 in the presence of WO_3, H_2O_2, and UV light (for the detailed experimental set-up see SI, (S2)). Typically, a 20 mg L^{-1} acid orange 7 solution was prepared in 50 mL of water. The pH was then adjusted to 2 by adding a 10% HCl solution. Afterwards, 40 mg L^{-1} of the WO_3 catalyst was added, and the suspension was stirred for 30 minutes under a 200 mL min^{-1} N_2 atmosphere to ensure sufficient adsorption–desorption equilibrium. Subsequently, 2 mL of 30% H_2O_2 was introduced and stirred for 5 minutes. The mixture was then irradiated using a 22 W UV lamp (approx.: 70 mW cm^{-2}, 365 nm). A 3 mL aliquot of the solution was collected, centrifuged to remove residual particles, and analyzed by UV-vis spectroscopy (JASCO V-570, Japan). Meanwhile, 0.5 mL of the evolved gas was sampled and injected into a gas chromatograph (GC – Shimadzu 2014, Japan) equipped with a thermal conductivity detector to identify gaseous products (detailed calibration procedures are provided in the SI, (S2)). For $^{\bullet}OH$ detection *via* the terephthalic acid fluorescence method, 0.04 g of the WO_3 catalyst was dispersed in a $\sim 4.8 \times 10^{-4}$ M terephthalic acid solution, followed by the addition of 2 mL of H_2O_2. The suspension was then irradiated under UV light. After irradiation, fluorescence intensity was measured using a fluorescence spectrophotometer (F-2700, Hitachi High-Technologies, Japan) at an excitation wavelength of 325 nm. For the scavenger experiments, two scavengers were employed: 0.059 mmol silver nitrate ($AgNO_3$) as an electron scavenger and 21 mmol *tert*-butanol as an $^{\bullet}OH$ radical scavenger. Each scavenger was added separately to the photo-Fenton-like reaction system, and the corresponding degradation performance was subsequently monitored.

3. Results and discussion

Fig. 1(a) illustrates the degradation of acid orange 7 under different reaction conditions. Under WO_3 with UV light and WO_3 with H_2O_2, there are no degradations observed, indicating that neither process alone facilitates a redox reaction. However, when H_2O_2 is exposed to UV light (H_2O_2 + UV), approximately 10% degradation occurs, likely due to the generation of hydroxyl radicals from H_2O_2 under UV irradiation.[26] In contrast,

a significant increase in degradation efficiency is observed when combining UV light, WO_3, and H_2O_2, reaching approximately 50% degradation. This strong degradation suggests a synergistic effect among UV light, WO_3, and H_2O_2.

The high degradation efficiency observed only in the presence of WO_3, UV light, and H_2O_2 has similarity with the photo-Fenton-like reaction, where Fe^{2+} reacts with H_2O_2 and UV light to accelerate hydroxyl radical generation.[26,27] Given this similarity, it is highly likely that a similar mechanism occurs in WO_3. To clarify this assumption, XPS analysis of the W 4f state before and after UV irradiation was performed, as shown in Fig. 1(b) and (c). The results reveal a gradual increase in the W^{5+} content from 2.5% to 3.6% after UV irradiation. This transition is also visually confirmed by the photographic evidence shown in Fig. 1(d), which shows a distinct color change from bright yellow to a greenish hue, attributed to the formation of W^{5+}, a phenomenon known as photochromism.[28,29]

The transition from W^{6+} to W^{5+} plays a crucial role in promoting the photo-Fenton-like reaction, as described by the following reaction pathway:

$$UV + WO_3 \rightarrow e^- + h^+ \quad (1)$$

$$e^- + W^{6+} \rightarrow W^{5+} \quad (2)$$

$$W^{5+} + H_2O_2 \rightarrow {}^{\bullet}OH + W^{6+} + OH^- \quad (3)$$

$$4h^+ + 2H_2O \rightarrow O_2 + 4H^+ \quad (4)$$

$$h^+ + OH^- \rightarrow {}^{\bullet}OH + H^+ \quad (5)$$

Under UV irradiation, WO_3 generates electron–hole pairs, where photogenerated electrons reduce W^{6+} to W^{5+} on the surface while holes on O 2p states are trapped at oxygen sites ready for promoting the possible chemical reaction.[30] The W^{5+} species then interact with H_2O_2, further promoting the formation of hydroxyl radicals which decompose acid orange 7 into carbon dioxide (direct evidence of CO_2 evolution has been shown in the SI, (S3)) and water, as illustrated in Fig. 1(e). Interestingly, the photo-Fenton-like activity of WO_3 shows better catalytic reaction than the traditional Fenton reaction either by using $FeCl_2$ ion and Fe_2O_3 nanoparticles as shown in Table 1 which highlight the strong potential of WO_3 as an effective material for waste-water degradation by photo-Fenton-like reactions.

While the electron continuously generates $^{\bullet}OH$ through a photo-Fenton like reaction process, holes in the valence band are ready to promote chemical reactions. There are two possible reactions for holes under these reaction conditions. The first one is the reaction with OH^- for generating $^{\bullet}OH$. This reaction is one of the common reactions for WO_3, where WO_3 has been acknowledged as a good oxidative photocatalyst.[31] However, based on the catalytic reaction process, if $^{\bullet}OH$ is formed, the degradation of acid orange 7 should occur even without H_2O_2. It indicates that the $^{\bullet}OH$ radicals are not formed under this reaction condition. The second possibility is the water oxidation process where holes directly oxidize water into O_2 and H^+.[19]

To confirm the second reaction possibility, oxygen evolution during the photo-Fenton-like reaction was investigated. To eliminate the possibility of O_2 release from direct H_2O_2 decomposition, a control experiment was conducted using

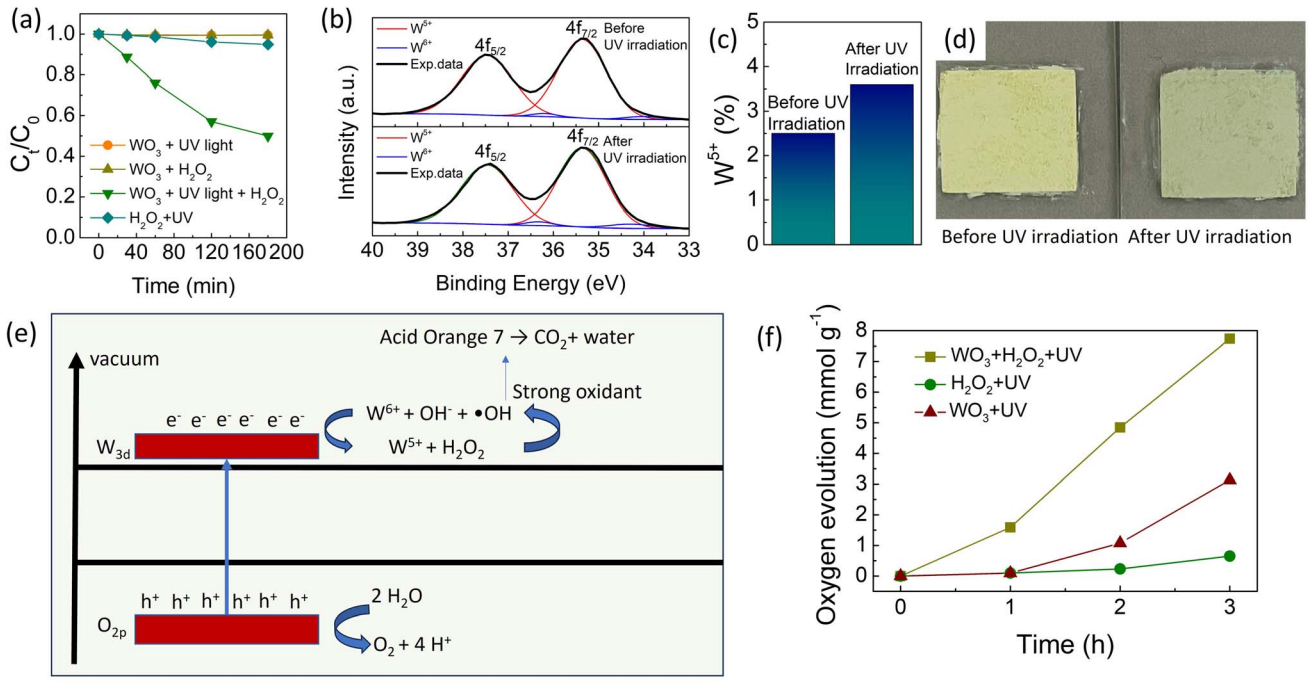

Fig. 1 (a) Acid orange 7 degradation under various systems. (b) XPS analysis of WO_3 before and after UV irradiation. (c) W^{5+} percentage obtained from XPS deconvolution. (d) Photographic images of WO_3 before and after reaction. (e) Proposed photo-Fenton reaction by using WO_3. (f) Oxygen evolution reaction by WO_3 + H_2O_2 + UV compared with WO_3 + UV and H_2O_2 + UV.

Table 1 Photocatalytic performance for acid orange 7 degradation and the oxygen evolution reaction of polaron WO_3 + H_2O_2 compared with other reports and data

Sample	Degradation rates (h^{-1})	Ref.	Sample	O_2 evolution rate (mmol g^{-1} h^{-1})	Ref.
Fe_2O_3 + H_2O_2	0.06	32	Fe + TiO_2	0.54	33
Fe_2O_3 + H_2O_2	0.13	34	Ag + TiO_2	0.06	35
Fe + H_2O_2	0.03	This work	FeOOH + WO_3 + H_2O_2	0.03	25
Polaron WO_3 + H_2O_2	0.18	This work	Polaron WO_3 + H_2O_2	1.62	This work

H_2O_2 under UV irradiation alone. The calibration details for the O_2 evolution reaction are provided in SI, (S2). As shown in Fig. 1(f), UV irradiation of H_2O_2 alone generates approximately 0.62 mmol g^{-1} of O_2, with an O_2 evolution rate of about 0.21 mmol g^{-1} h^{-1}. In the presence of WO_3 under UV irradiation, the O_2 production increases significantly to 3.1 mmol g^{-1}, confirming the enhanced photocatalytic activity. To exclude the contribution from H_2O_2 photodecomposition, the O_2 evolution rates were corrected by subtracting 0.21 mmol g^{-1} h^{-1}. After correction, the O_2 evolution rate for WO_3 under UV irradiation is approximately 0.80 mmol g^{-1} h^{-1} and further increases to about 1.62 mmol g^{-1} h^{-1} when WO_3 is combined with H_2O_2 (see SI, (S4)). These results demonstrate that both photogenerated electrons and holes in WO_3 are effectively utilized, overcoming the previously reported limitations associated with WO_3 photocatalysis. Furthermore, the O_2 evolution performance achieved in this work is higher than values reported in the literature (Table 1), reinforcing the enhanced photo-Fenton-like activity of WO_3.

The WO_3-based photo-Fenton-like reaction has been demonstrated; however, the degradation efficiency remains relatively low (50% in 180 minutes). Therefore, further optimization strategies are necessary. The key to enhancing the photo-Fenton-like activity in WO_3 lies in the generation of W^{5+} species. Increasing the formation of W^{5+} under UV irradiation is essential. Previous studies have proposed that defect engineering can play a crucial role in promoting W^{5+} generation,[36] such as hydrogen annealing[37] or doping,[38–40] and can improve photochromism. However, these approaches introduce additional processing steps and materials, reducing overall efficiency.

Different from the above-mentioned techniques, the control of the nucleation and growth process during synthesis also provides a controllable lattice behavior including strain and defect, which is insightful for improving W^{5+} formation in WO_3. In this study, W^{5+} formation was improved by regulating crystal growth through modulating the protonation level during synthesis. The proton concentration varied from $[H^+] = 0.8$, 1.6, 2.8 and 5.7. Initially the precursors are still in the form of (H_4WO_5) (see XRD and TEM results in SI, (S5)) and the particle size of the precursor decreases as the protonation increases, indicating the increase of the supersaturation degree due to high protonation. After annealing treatment, stable WO_3 is formed (detailed structure analysis shown in Fig. 4(a) and (b)). The change in the acid concentration significantly affects W^{5+} formation in the WO_3 structure. Fig. 2(a) shows images of WO_3 at different protonation levels after UV irradiation. Clear evidence demonstrates that after UV irradiation, the color gradually changed to dark green as protonation increased, indicating an enhancement in W^{5+} generation. XPS analysis of W 4f after and before UV irradiation has confirmed that the W^{5+} gradually increases with increasing protonation level from $[H^+]$ 0.8 to 5.7 (Fig. 2(b)). Table 2 also shows the details of W^{5+} percentages after UV irradiation which indicates a gradual increase with the increase of protonation. Besides W^{5+} formation, the N_2 adsorption desorption analysis results (Fig. 2(c)) have revealed that the high protonation also increases the surface area, pore size and pore volumes of WO_3 as tabulated in Table 2.

The influence of increasing protonation was further evaluated through the photo-Fenton reaction. Fig. 2(d) and (e) presents the acid orange 7 degradation profiles at different protonation levels. The degradation efficiency of WO_3 increases progressively with higher protonation, with the reaction rate rising from 0.18 to 0.68 h^{-1}. This trend clearly indicates that protonation enhances the photo-Fenton-like activity. At this stage, two major factors appear to affect the photo-Fenton-like performance: (i) the formation of W^{5+} species and (ii) the changes in surface properties. To clarify their respective contributions, several additional analyses were performed. First, the adsorption of acid orange 7 on WO_3 was examined to evaluate the influence of surface characteristics. As shown in the SI, (S6), acid orange 7 adsorption increases slightly with increasing surface area, with approximately 5% removal observed. This indicates that surface properties also contribute to the degradation process. This conclusion is further supported by the surface charge analysis and photo-Fenton-like reactions performed at different pH values (SI, (S7)) where the surface charge and type of pollutant affected the photo-Fenton-like reactions, both of which confirm that surface characteristics play a role in accelerating the photo-Fenton-like reaction. On the other hand, to assess the contribution of W^{5+} species, photo-Fenton-like reactions were conducted using samples with comparable surface areas but different internal defect (W^{5+}) concentrations by heating the $[H^+] = 5.7$ precursor under air and a nitrogen atmosphere (see SI, (S8)). The results clearly show that the higher W^{5+} significantly enhances the degradation rate although the surface area was nearly similar. Taken together, these data demonstrate that the improved photo-Fenton-like performance arises from the synergistic effect between increased formation of W^{5+} and the enhancement of surface properties induced by protonation. While surface

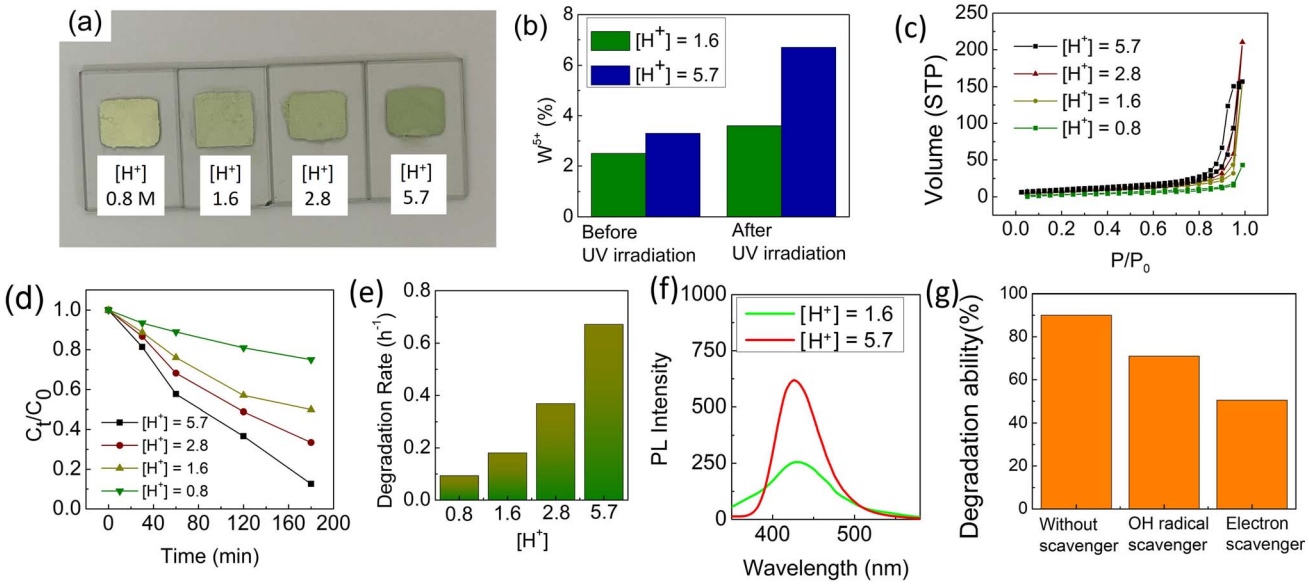

Fig. 2 (a) Photographic images of WO_3 samples with different protonation levels after UV irradiation. (b) W^{5+} percentages before and after UV irradiation, obtained from XPS analysis of the W 4f region. (c) N_2 adsorption–desorption isotherms of WO_3 samples with different protonation levels. (d) Acid orange 7 degradation profiles for WO_3 samples with varying protonation. (e) Degradation rate constants for acid orange 7 using WO_3 with different protonation levels. (f) Fluorescence analysis using terephthalic acid to detect $^{\bullet}OH$ radical generation for $[H^+] = 1.6$ and 5.7, and (g) scavenger tests using $^{\bullet}OH$ scavengers and electron scavengers.

properties mainly influence the attachment of acid orange 7 onto WO_3, the formation of W^{5+} is primarily responsible for promoting the conversion of H_2O_2 into $^{\bullet}OH$ radicals.

Fig. 2(f) presents the terephthalic acid fluorescence analysis, confirming $^{\bullet}OH$ generation under irradiation. The samples with higher protonation exhibit the highest fluorescence intensity, indicating enhanced $^{\bullet}OH$ production which correlated with improvement of acid orange 7 degradation. However, although $^{\bullet}OH$ plays a key role in acid orange 7 degradation, the initial process started from the photoexcitation of electrons that generate W^{5+}, which then reacts with H_2O_2 to produce $^{\bullet}OH$ radicals. This conclusion is further supported by the scavenger experiments shown in Fig. 2(g), where the presence of electron scavengers results in the greatest suppression of catalytic activity, clearly demonstrating that electron-driven polaron formation is the major contributor to the overall reaction.

To assess the potential of this photo-Fenton-like reaction by applications, the degradation of other types of pollutants was also investigated (Fig. 3(a)). Cationic dyes, represented by methylene blue, and pharmaceutical waste, represented by 4-nitrophenol, were studied. The results show that the photo-Fenton-like reaction using WO_3 with high W^{5+} is effective in degrading various types of pollutants, demonstrating its potential for future wastewater management applications.

The improvement of electron site efficiency is directly correlated with the improvement in the hole efficiency. As shown in Fig. 3(b), the OER rate increases steadily from 1.62 mmol g^{-1} h^{-1} to 3.66 mmol g^{-1} h^{-1}. These data demonstrate a clear correlation between the enhanced photo-Fenton-like reaction, driven by an increase in W^{5+} attributed to the increase of protonation. However, as shown in the mechanism section, Fig. 1(e), the recycling process should occur during reaction which means that WO_3 should have good recyclability to be used several times. For clarifying these phenomena, the repeatability test was also conducted to assess the recyclability of the photo-Fenton-like reaction. The data plotted in Fig. 3(c) show the good stability of the oxygen evolution reaction and dye degradation after 4 recycle experiments which further elevated the potential of this concept for practical applications. This stability test confirmed the advantages of the photo-Fenton like reaction by using WO_3 which shows better catalytic stability compared to traditional iron ion, TiO_2,[13] CuO,[14] and Mn_3O_4.[15]

Table 2 W^{5+} concentration and physical surface properties of WO_3 at different protonation levels

Sample	W^{5+}% after irradiation	Surface area (m^2 g^{-1})	Pore size (nm)	Pore volume (cc g^{-1})
$[H^+] = 0.8$	2.2	15	3.061	0.066
$[H^+] = 1.6$	3.6	24	2.178	0.244
$[H^+] = 2.8$	5.5	29	29.47	0.331
$[H^+] = 5.7$	6.7	37	32.50	0.247

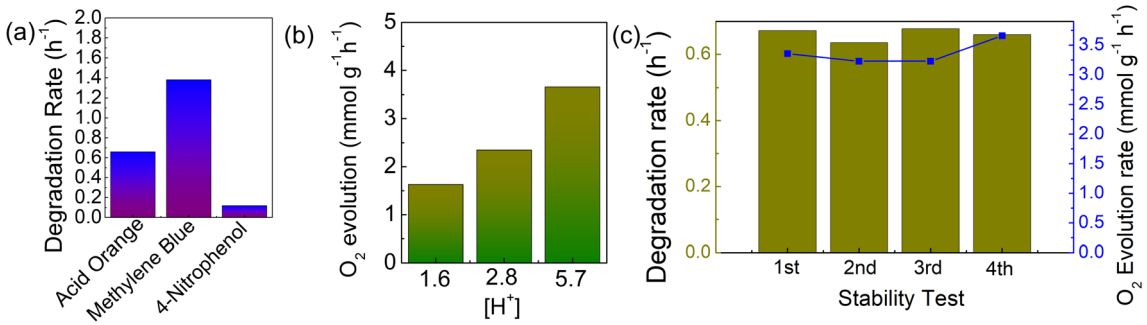

Fig. 3 (a) Degradation ability of the $[H^+] = 5.7$ sample for degrading other types of wastewaters. (b) Oxygen evolution rate for different protonation samples. (c) Stability of the $[H^+] = 5.7$ catalysts in terms of the reaction rate for acid orange 7 removal and the oxygen evolution reaction.

The enhancement of the photo-Fenton-like reaction has been clarified with relatively satisfactory results through increasing protonation. However, the origin of the increase in surface area and W^{5+} formation during UV irradiation, along with the gradual increase in protonation, needs to be clarified in detail. One major question is clarifying the crystal growth behavior at different protonation levels, which affects the ease of W^{5+} formation and surface properties. Initially, XRD patterns were analyzed to investigate the crystal structure of WO_3 at different protonation levels. As shown in Fig. 4(a), the diffraction patterns exhibit the characteristic peaks corresponding to monoclinic WO_3 (JCPDS no. 83-0950) with a space group of $P2_1/n$. Rietveld refinement performed using the Profex (open-source) software confirms that all patterns can be well-fitted with a single WO_3 phase, indicating the absence of any secondary phases. No diffraction peaks associated with H_4WO_5 were detected in any of the samples. SI (S9) further shows that at 400 °C, H_4WO_5 is fully transformed into the WO_3 structure.

Although all samples crystallize in the monoclinic WO_3 phase, the intensity of the (002) reflection decreases progressively with increasing protonation (inset of Fig. 4(b)). The intensity ratio of the (002) to (200) planes decrease sharply from 2.33 for $[H^+] = 0.8$ to 0.33 for $[H^+] = 5.7$, indicating a significant change in the relative growth orientation associated with protonation. The (002) peak is usually correlated with the lateral dimension of the material. With the gradual decrease in the (002) peak, there is a possibility that the lateral dimension also decreases, indicating a reduction in particle size as confirmed by TEM analysis (Fig. 4(c) and (d)) attributed to the increase in supersaturation degree which increases the number of nuclei formations and decreases the particle growth. It is easy to understand that this smaller size correlated with surface area enhancement. On the

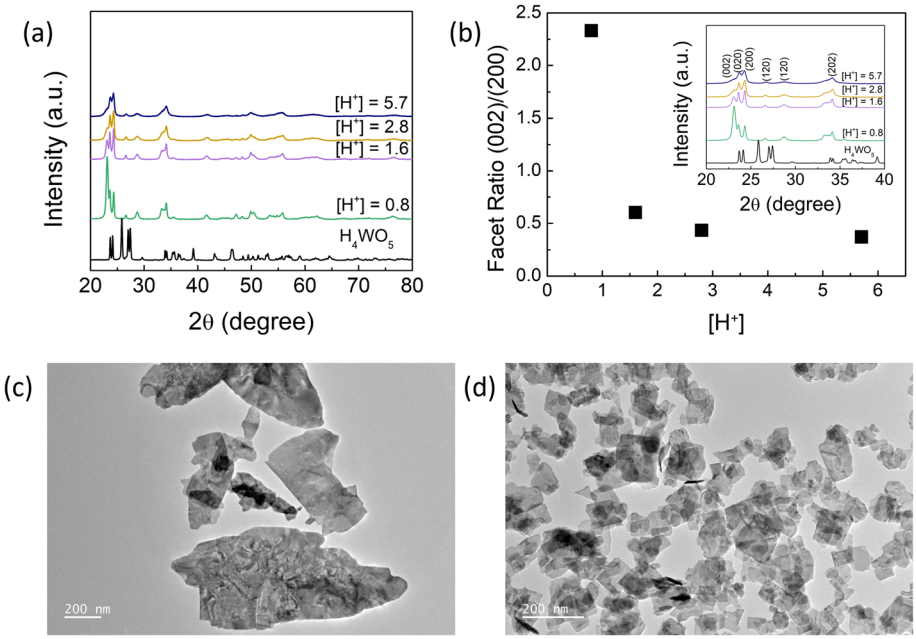

Fig. 4 (a) XRD spectra of WO_3 prepared at different protonation levels. (b) Intensity ratio between the (002) facet with the (200) facet (inset shows XRD spectra of WO_3 prepared at different protonation levels with narrow angle ranges). TEM images of WO_3 for (c) $[H^+] = 0.8$ and (d) $[H^+] = 5.7$ samples.

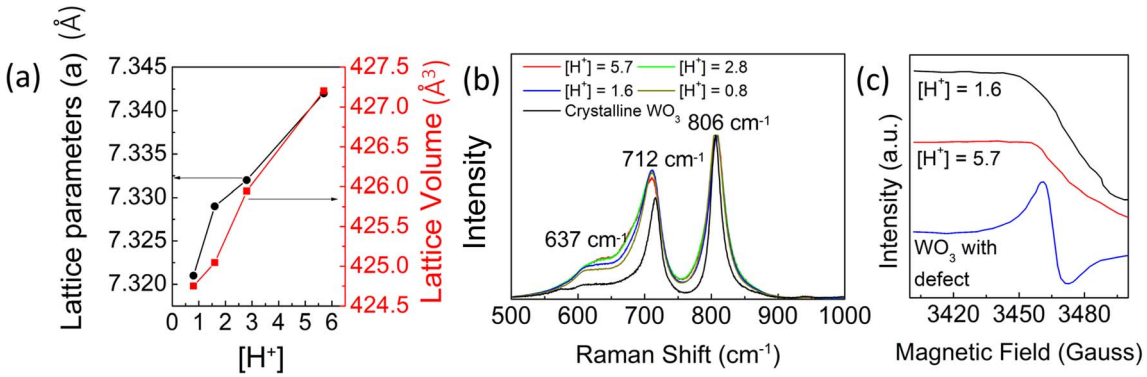

Fig. 5 (a) Lattice parameters analysis of WO_3 with different protonation levels. (b) Raman spectra of WO_3 prepared at different protonation levels. (c) EPR analysis of WO_3 for $[H^+] = 1.6$, $[H^+] = 5.7$, and defect (vacancy) containing WO_3.

other hand, to find the origin of high W^{5+} formation during UV irradiation, additional analysis is required.

The detailed crystal structure analysis at different protonation levels was then performed by examining the changes in lattice volume and lattice parameters, as shown in Fig. 5(a). An expansion in lattice volume was observed with increasing supersaturation degree attributed to the different protonation levels during synthesis. The lattice strain was then estimated by comparing the lattice structure of high crystalline WO_3 with the current samples (see SI, (S10)). The results show that with higher protonation, an increase in the tensile strain from 0.21% to 0.79% is observed. The expansion of the lattice might be correlated with the distortion of the lattice crystals by protonation. For confirming the distortion in the crystal, Raman spectroscopy was performed to analyze the chemical bonding between tungsten and oxygen atoms (Fig. 5(b)). Two distinct peaks were observed in the range of 500–1000 cm^{-1} at 806 cm^{-1} and 712 cm^{-1}, corresponding to the stretching vibrations of W–O–W bonds.[41,42] Notably, peak broadening at 712 cm^{-1} became more pronounced with increasing protonation, indicating increased lattice distortion. Additionally, a shoulder peak at 637 cm^{-1} emerged and intensified with higher protonation levels. This feature, absent in highly crystalline WO_3, further confirms the progressive distortion of the crystal structure with increasing protonation.

The origin of lattice distortion can be attributed to several factors, including strain and oxygen vacancy defects. To determine the primary cause, electron paramagnetic resonance (EPR) analysis was performed on WO_3 samples with different protonation levels to confirm the formation of lattice defects (vacancies) (Fig. 5(c)). Additionally, defective WO_3 was provided as a comparison to confirm the presence of oxygen vacancies by annealing the $[H^+] = 5.7$ under a N_2 atmosphere for 400 °C for 2 h. A distinct signal was observed at 3450–3480 gauss, characteristic of oxygen vacancy formation. However, no corresponding oxygen vacancy signals were detected for WO_3 samples with $[H^+] = 1.6$ and $[H^+] = 5.7$. Instead, distortion is likely induced by strain attributed to the rapid supersaturation degree where at high supersaturation rapid nucleation occurs, which limits crystal growth and introduces structural disorder.

The strain-modulated enhancement of W^{5+} formation and its influence on the reaction process have been confirmed. However, the precise origin of the strain effect on W^{5+} formation remains unclear. Several researchers have suggested that strain can induce electron localization, allowing electrons to remain longer on the surface.[23,43,44] This phenomenon was further validated in the case of WO_3. As shown in the photoluminescence analysis (SI, (S11)), the peak intensity at $[H^+] = 5.7$ is lower than that at $[H^+] = 1.6$, indicating that electrons spend more time in the conduction band, thereby promoting polaron formation. Enhanced electron localization due to strain was also confirmed by spin-polarized density functional theory calculations, which revealed an increase in total magnetization from 2.83μ_B in the unstrained structure to 3.14μ_B in the strained structure (SI, (S12)). Collectively, these results demonstrate that strained WO_3 more readily localizes electrons and promotes polaronic behavior, thereby accelerating the photo-Fenton-like reaction.

4. Conclusion

In this study, a novel concept has been successfully introduced for the utilization of charge carriers in WO_3 through a photo-Fenton-like reaction. Light irradiation of WO_3 promotes the excitation of electrons, reducing W^{6+} to W^{5+}, which interacts with H_2O_2 to produce $^{\bullet}OH$ that was successfully utilized for wastewater remediation. However, the holes in the valence band efficiently conduct water splitting to produce O_2, attributed to the trapping of electrons that promotes the photo-Fenton-like reaction. The photo-Fenton-like reaction was optimized by controlling protonation during synthesis, which regulates crystal growth. Higher protonation resulted in smaller particle sizes, larger surface areas, and increased W^{5+} content, attributed to the higher crystal strain. These changes in physical and electronic properties enhance the ability of WO_3 to drive the photo-Fenton-like reaction for acid orange 7 degradation and the oxygen evolution reaction, owing to the synergistic effect between surface chemistry and W^{5+} formation. Overall, these findings demonstrate the efficient charge utilization of WO_3 in photo-Fenton-like processes.

Author contributions

The manuscript was written through contributions of all authors. All authors have given approval to the final version of the manuscript.

Conflicts of interest

There are no conflicts to declare.

Data availability

The data supporting this article have been included as part of the supplementary information (SI). Supplementary information is available. See DOI: https://doi.org/10.1039/d5ta07868g.

Acknowledgements

The authors acknowledge the support from the Japan Science and Technology Agency (JST) [MIRAI, Grant Number JPMJMI17E4 and CREST, Grant Number JPMJCR16P3], the New Energy and Industrial Technology Development Organization of Japan (NEDO), JSPS KAKENHI (Grant Numbers JP16H06367, JP20K20548, and JP21H05010), Materials Processing Science Project (Materealize; Grant Number JPMXP0219192801) of the Ministry of Education, Culture, Sports, Science and Technology (MEXT), Professional Development Consortium for Computational Materials Scientists (PCoMS), and the World Premier International Research Center Initiative (WPI), MEXT, Japan. The Analytical Research Core for Advanced Materials, Institute for Materials Research, Tohoku University is acknowledged for JEM2100Plus measurement. The authors appreciate the Central Analytical Facility (CAF), IMRAM, Tohoku University for providing the EPR facility.

References

1 Q. Chen, F. Lü, J. Qiu, H. Zhang and P. He, Pathways and Selectivity of Fenton Degradation of Different Precursor Species of Dissolved Organic Matter, *Nat. Commun.*, 2025, **16**, 61753, DOI: 10.1038/s41467-025-61753-7.

2 M. Huang, H. Z. Liu, Q. Q. Huang, T. Zhou, X. Wu, W. W. Li and H. Q. Yu, Self-Activated Heterogeneous Fenton Process for Accelerated Degradation of Aromatic Pollutants over Copper Oxide Catalysts, *Angew. Chem., Int. Ed.*, 2025, **64**(30), e202508754, DOI: 10.1002/anie.202508754.

3 Q. Yan, C. Lian, K. Huang, L. Liang, H. Yu, P. Yin, J. Zhang and M. Xing, Constructing an Acidic Microenvironment by MoS_2 in Heterogeneous Fenton Reaction for Pollutant Control, *Angew. Chem., Int. Ed.*, 2021, **60**(31), 17155–17163, DOI: 10.1002/anie.202105736.

4 V. Manikandan, D. Elango, V. Subash, P. Kumar, J. S. Packialakshmi, P. Jayanthi, Y. J. Sun and K. S. Song, Needle ZrO_x Loaded $NiFe_2O_4$ Catalysts for Photo-Fenton Degradation of Bisphenol A and 4 Nitrophenol, *npj Clean Water*, 2025, **8**, 50, DOI: 10.1038/s41545-025-00483-1.

5 S. A. Walling, W. Um, C. L. Corkhill and N. C. Hyatt, Fenton and Fenton-like Wet Oxidation for Degradation and Destruction of Organic Radioactive Wastes, *npj Mater. Degrad.*, 2021, **5**, 50, DOI: 10.1038/s41529-021-00192-3.

6 M. M. Zareh, A. S. El-Sayed and D. M. El-Hady, Biosorption Removal of Iron from Water by Aspergillus Niger, *npj Clean Water*, 2022, **5**, 58, DOI: 10.1038/s41545-022-00201-1.

7 T. Liu, K. Hu, Y. Li, Y. Wang, D. Han, Z. Wang and F. Gu, The Z-Scheme MIL-88B(Fe)/BiOBr Heterojunction Promotes Fe(III)/Fe(II) Cycling and Photocatalytic-Fenton-Like Synergistically Enhances the Degradation of Ciprofloxacin, *Small*, 2024, **20**, 2309541, DOI: 10.1002/smll.202309541.

8 Y. Song, C. Rong, J. Shang, Y. Wang, Y. Zhang and K. Yu, Synthesis of an Inorganic-Framework Molecularly Imprinted Fe-Doped TiO_2 Composite and Its Selective Photo-Fenton-like Degradation of Acid Orange II, *J. Chem. Technol. Biotechnol.*, 2017, **92**(8), 2038–2049, DOI: 10.1002/jctb.5199.

9 Z. Wu, Z. Xiong, B. Huang, G. Yao, S. Zhan and B. Lai, Long-Range Interactions Driving Neighboring Fe–N_4 Sites in Fenton-like Reactions for Sustainable Water Decontamination, *Nat. Commun.*, 2024, **15**, 7775, DOI: 10.1038/s41467-024-52074-2.

10 J. Yan, L. Qian, W. Gao, Y. Chen, D. Ouyang and M. Chen, Enhanced Fenton-like Degradation of Trichloroethylene by Hydrogen Peroxide Activated with Nanoscale Zero Valent Iron Loaded on Biochar, *Sci. Rep.*, 2017, **7**, 43051, DOI: 10.1038/srep43051.

11 Y. Zhu, S. Qiu, W. Tang, F. Deng, F. Ma, Y. Zheng and H. Xie, Sustainable Fe^{3+} Reduction by Fe_3O_4@tourmaline in Fenton-like System, *Chem. Eng. J.*, 2022, **437**, 135480, DOI: 10.1016/j.cej.2022.135480.

12 X. Huang, H. Zhou, X. Yue, S. Ran and J. Zhu, Novel Magnetic Fe_3O_4/α-FeOOH Nanocomposites and Their Enhanced Mechanism for Tetracycline Hydrochloride Removal in the Visible Photo-Fenton Process, *ACS Omega*, 2021, **6**(13), 9095–9103, DOI: 10.1021/acsomega.1c00204.

13 J.-y. Qiu, J.-h. Chen, B.-y. Xiao, X.-x. Li, T. Wan, F.-h. Qin, Y. Mi and Z.-y. Huang, Oxygen Deficient TiO_{2-x} with Dual Reaction Sites for Activation of H_2O_2 to Degrade Organic Pollutants, *Catal. Lett.*, 2020, **150**(1), 222–233, DOI: 10.1007/s10562-019-02920-6.

14 M. Fang, R. Zheng, Y. Wu, D. Yue, X. Qian, Y. Zhao and Z. Bian, CuO Nanosheet as a Recyclable Fenton-like Catalyst Prepared from Simulated Cu(II) Waste Effluents by Alkaline H_2O_2 Reaction, *Environ. Sci.: Nano*, 2019, **6**(1), 105–114, DOI: 10.1039/c8en00930a.

15 Z. Weng, J. Li, Y. Weng, M. Feng, Z. Zhuang and Y. Yu, Surfactant-Free Porous Nano-Mn_3O_4 as a Recyclable Fenton-like Reagent That Can Rapidly Scavenge Phenolics without H_2O_2, *J. Mater. Chem. A*, 2017, **5**(30), 15650–15660, DOI: 10.1039/c7ta04042c.

16 J. Ortiz, D. Acosta and C. Magaña, Long-Term Cycling and Stability of Crystalline WO_3 Electrochromic Thin Films Prepared by Spray Pyrolysis, *J. Solid State Electrochem.*, 2022, **26**(8), 1667–1676, DOI: 10.1007/s10008-022-05211-0.

17 J. Tao and T. Liu, Electron and Hole Polaron Formation and Transport in Monoclinic WO_3 Studied by Hybrid Functional Approach, *J. Phys. Chem. C*, 2023, **127**(32), 16204–16210, DOI: 10.1021/acs.jpcc.3c03991.

18 H. Hassani, E. Bousquet, X. He, B. Partoens and P. Ghosez, The Anti-Distortive Polaron as an Alternative Mechanism for Lattice-Mediated Charge Trapping, *Nat. Commun.*, 2025, **16**, 1688, DOI: 10.1038/s41467-025-56791-0.

19 H. Suzuki, O. Tomita, M. Higashi and R. Abe, Tungstic Acids H_2WO_4 and H_4WO_5 as Stable Photocatalysts for Water Oxidation under Visible Light, *J. Mater. Chem. A*, 2017, **5**(21), 10280–10288, DOI: 10.1039/c7ta01228d.

20 X. Zhang, A. Yoko, Y. Zhou, W. Jee, A. Mayoral, T. Liu, J. Guan, Y. Lu, T. W. Keal, J. Buckeridge, K. Ninomiya, M. Nishibori, S. Yamamoto, I. Matsuda, T. Adschiri, O. Terasaki, S. M. Woodley, C. R. A. Catlow and A. A. Sokol, Surface-Driven Electron Localization and Defect Heterogeneity in Ceria, *J. Am. Chem. Soc.*, 2025, **147**, 33888–33902, DOI: 10.1021/jacs.5c10679.

21 X. Hao, A. Yoko, C. Chen, K. Inoue, M. Saito, G. Seong, S. Takami, T. Adschiri and Y. Ikuhara, Atomic-Scale Valence State Distribution inside Ultrafine CeO_2 Nanocubes and Its Size Dependence, *Small*, 2018, **14**, 1802915, DOI: 10.1002/smll.201802915.

22 X. Hao, A. Yoko, K. Inoue, Y. Xu, M. Saito, C. Chen, G. Seong, T. Tomai, S. Takami, A. L. Shluger, B. Xu, T. Adschiri and Y. Ikuhara, Atomistic Origin of High-Concentration Ce^{3+} in {100}-Faceted Cr-Substituted CeO_2 Nanocrystals, *Acta Mater.*, 2021, **203**, 116473, DOI: 10.1016/j.actamat.2020.11.015.

23 A. Yoko, Y. Omura, K. Ninomiya, M. Nishibori, T. Fujita, H. Kasai, E. Nishibori, N. Chiba, G. Seong, T. Tomai and T. Adschiri, Fusion Growth and Extraordinary Distortion of Ultrasmall Metal Oxide Nanoparticles, *J. Am. Chem. Soc.*, 2024, **146**(23), 16324–16331, DOI: 10.1021/jacs.4c05106.

24 Z. Yuan, H. Miao, Z. Jiang, X. Zhao, S. Shi and X. Zhu, Oxygen Vacancy Activated Inlaid Fe Active Sites in WO_3 for Sustainable and Efficient Photo-Fenton Oxidation in a Wide PH Range, *Mol. Catal.*, 2025, **577**, 114962, DOI: 10.1016/j.mcat.2025.114962.

25 J. Yang, J. Hao, J. Wei, J. Dai and Y. Li, Visible-Light-Driven Selective Oxidation of Methane to Methanol on Amorphous FeOOH Coupled m-WO_3, *Fuel*, 2020, **266**, 117104, DOI: 10.1016/j.fuel.2020.117104.

26 L. Yu, J. Chen, Z. Liang, W. Xu, L. Chen and D. Ye, Degradation of Phenol Using Fe_3O_4-GO Nanocomposite as a Heterogeneous Photo-Fenton Catalyst, *Sep. Purif. Technol.*, 2016, **171**, 80–87, DOI: 10.1016/j.seppur.2016.07.020.

27 R. Saleh and A. Taufik, Degradation of Methylene Blue and Congo-Red Dyes Using Fenton, Photo-Fenton, Sono-Fenton, and Sonophoto-Fenton Methods in the Presence of Iron(II,III) Oxide/Zinc Oxide/Graphene (Fe_3O_4/ZnO/Graphene) Composites, *Sep. Purif. Technol.*, 2019, **210**, 563–573, DOI: 10.1016/j.seppur.2018.08.030.

28 S. Wang, W. Fan, Z. Liu, A. Yu and X. Jiang, Advances on Tungsten Oxide Based Photochromic Materials: Strategies to Improve Their Photochromic Properties, *J. Mater. Chem. C*, 2018, 191–212, DOI: 10.1039/c7tc04189f.

29 J. Wei, X. Jiao, T. Wang and D. Chen, The Fast and Reversible Intrinsic Photochromic Response of Hydrated Tungsten Oxide Nanosheets, *J. Mater. Chem. C*, 2015, **3**(29), 7597–7603, DOI: 10.1039/c5tc01350j.

30 S. Zeb, G. Sun, Y. Nie, H. Xu, Y. Cui and X. Jiang, Advanced Developments in Nonstoichiometric Tungsten Oxides for Electrochromic Applications, *Mater. Adv.*, 2021, 6839–6884, DOI: 10.1039/d1ma00418b.

31 Z. Wang and H. Einaga, WO_3-Based Materials for Photocatalytic and Photoelectrocatalytic Selective Oxidation Reactions, *ChemCatChem*, 2023, **15**, e202300723, DOI: 10.1002/cctc.202300723.

32 K. Lin, S. Afzal, L. Xu, T. Ding, F. Li and M. Zhang, Heterogeneous Photo-Fenton Degradation of Acid Orange 7 Activated by Red Mud Biochar under Visible Light Irradiation, *Environ. Pollut.*, 2023, **327**, 121454, DOI: 10.1016/j.envpol.2023.121454.

33 M. J. Sampaio, Z. Yu, J. C. Lopes, P. B. Tavares, C. G. Silva, L. Liu and J. L. Faria, Light-Driven Oxygen Evolution from Water Oxidation with Immobilised TiO_2 Engineered for High Performance, *Sci. Rep.*, 2021, **11**, 21306, DOI: 10.1038/s41598-021-99841-5.

34 J. Zheng, Z. Gao, H. He, S. Yang and C. Sun, Efficient Degradation of Acid Orange 7 in Aqueous Solution by Iron Ore Tailing Fenton-like Process, *Chemosphere*, 2016, **150**, 40–48, DOI: 10.1016/j.chemosphere.2016.02.001.

35 J. Ke, H. Zhou, J. Liu, X. Duan, H. Zhang, S. Liu and S. Wang, Crystal Transformation of 2D Tungstic Acid H_2WO_4 to WO_3 for Enhanced Photocatalytic Water Oxidation, *J. Colloid Interface Sci.*, 2018, **514**, 576–583, DOI: 10.1016/j.jcis.2017.12.066.

36 Z. F. Huang, J. Song, L. Pan, X. Zhang, L. Wang and J. J. Zou, Tungsten Oxides for Photocatalysis, Electrochemistry, and Phototherapy, *Adv. Mater.*, 2015, **27**, 5309–5327, DOI: 10.1002/adma.201501217.

37 J. Zhu, M. Vasilopoulou, D. Davazoglou, S. Kennou, A. Chroneos and U. Schwingenschlögl, Intrinsic Defects and H Doping in WO_3, *Sci. Rep.*, 2017, **7**, 40882, DOI: 10.1038/srep40882.

38 H. Miyazaki, M. Inada, H. Suzuki and T. Ota, Fabrication of WO_3-Based Composite Films and Improvement Its Photochromic Properties by Copper Doping, *Bull. Chem. Soc. Jpn.*, 2012, **85**(9), 1053–1056, DOI: 10.1246/bcsj.20120130.

39 H. Miyazaki, M. Inada, H. Suzuki and T. Ota, Molybdenum Doping Effects on Photochromic Properties of WO_3 Based Composite Films, *J. Ceram. Soc. Jpn.*, 2013, **121**(1), 106–108.

40 K. Syrek, S. Kotarba, M. Zych, M. Pisarek, T. Uchacz, K. Sobańska, L. Pięta and G. D. Sulka, Surface Engineering of Anodic WO_3 Layers by In Situ Doping for Light-Assisted Water Splitting, *ACS Appl. Mater. Interfaces*, 2024, **16**, 36752–36762, DOI: 10.1021/acsami.4c02927.

41 J. Wei, X. Jiao, T. Wang and D. Chen, The Fast and Reversible Intrinsic Photochromic Response of Hydrated Tungsten

Oxide Nanosheets, *J. Mater. Chem. C*, 2015, **3**(29), 7597–7603, DOI: 10.1039/c5tc01350j.

42 C. Santato, M. Odziemkowski, M. Ulmann and J. Augustynski, Crystallographically Oriented Mesoporous WO_3 Films: Synthesis, Characterization, and Applications, *J. Am. Chem. Soc.*, 2001, **123**(43), 10639–10649, DOI: 10.1021/ja011315x.

43 S. Yan, C. Peng, C. Yang, Y. Chen, J. Zhang, A. Guan, X. Lv, H. Wang, Z. Wang, T. K. Sham, Q. Han and G. Zheng, Electron Localization and Lattice Strain Induced by Surface Lithium Doping Enable Ampere-Level Electrosynthesis of Formate from CO_2, *Angew. Chem., Int. Ed.*, 2021, **60**(49), 25741–25745, DOI: 10.1002/anie.202111351.

44 A. F. Zinovieva, V. A. Zinovyev, A. V. Nenashev, L. V. Kulik and A. V. Dvurechenskii, Electron Spatial Localization Tuned by Strain in Ge/Si Quantum Dot Heterostructures, *Phys. Rev. B*, 2019, **99**, 115314, DOI: 10.1103/PhysRevB.99.115314.

